International Journal of Minerals, Metallurgy and Materials
Volume 30, Number 2, February 2023, Page 324
https://doi.org/10.1007/s12613-021-2355-6

Influence of rare earth Ce on hot deformation behavior of as-cast Mn18Cr18N high nitrogen austenitic stainless steel

Yushuo Li[1)], *Yanwu Dong*[1,2),✉], *Zhouhua Jiang*[1,2),✉], *Qingfei Tang*[1)], *Shuyang Du*[1)], *and Zhiwen Hou*[1)]

1) School of Metallurgy, Northeastern University, Shenyang 110819, China
2) State Key Laboratory of Rolling and Automation, Northeastern University, Shenyang 110819, China
(Received: 25 June 2021; revised: 16 September 2021; accepted: 18 September 2021)

Abstract: The hot deformation behavior of Mn18Cr18N and Mn18Cr18N+Ce high nitrogen austenitic stainless steels at 1173–1473 K and 0.01–1 s^{-1} were investigated by thermal compression tests. The influence mechanism of Ce on the hot deformation behavior was analyzed by Ce-containing inclusions and segregation of Ce. The results show that after the addition of Ce, large, angular, hard, and brittle inclusions (TiN–Al_2O_3, TiN, and Al_2O_3) can be modified to fine and dispersed Ce-containing inclusions (Ce–Al–O–S and TiN–Ce–Al–O–S). During the solidification, Ce-containing inclusions can be used as heterogeneous nucleation particles to refine as-cast grains. During the hot deformation, Ce-containing inclusions can pin dislocation movement and grain boundary migration, induce dynamic recrystallization (DRX) nucleation, and avoid the formation and propagation of micro cracks and gaps. In addition, during the solidification, Ce atoms enrich at the front of solid–liquid interface, resulting in composition supercooling and refining the secondary dendrites. Similarly, during the hot deformation, Ce atoms tend to segregate at the boundaries of DRX grains, inhibiting the growth of grains. Under the synergistic effect of Ce-containing inclusions and Ce segregation, although the hot deformation resistance and hot deformation activation energy are improved, DRX is more likely to occur and the size of DRX grains is significantly refined, and the problem of hot deformation cracking can be alleviated. Finally, the microhardness of the samples was measured. The results show that compared with as-cast samples, the microhardness of hot-deformed samples increases significantly, and with the increase of DRX degree, the microhardness decreases continuously. In addition, Ce can affect the microhardness of Mn18Cr18N steel by affecting as-cast and hot deformation microstructures.

Keywords: rare earth; hot deformation; Mn18Cr18N steel; non-metallic inclusions; element segregation; microhardness

1. Introduction

With the rapid development of steam turbine generator industry, the capacity of generating units is increasing, and requirements for the quality of generating units are getting higher and higher. The retaining ring is an important component of generating units, whose core function is to prevent the displacement and eccentricity of the rotor winding, and to protect the rotor winding [1–3], thus the retaining ring steel must have high yield strength and good plastic toughness. Besides, it is necessary to prevent excessive temperature caused by magnetic flux leakage and eddy current, so the retaining ring steel also needs to meet the requirement of non-magnetism. Non-magnetic Mn18Cr18N high nitrogen austenitic stainless steel is a suitable material, but its manufacturing process is complicated, especially hot forging. The forging range of Mn18Cr18N steel is very narrow and it is easy to be cracked [4–6].

In order to solve the problem of hot working cracking and prepare Mn18Cr18N steel with fine and uniform grains, researchers have done many studies on the hot deformation behavior of retaining ring steel, including movement and evolution mechanisms of dislocations, nucleation and growth mechanisms of DRX grains, reasonable hot deformation parameters, etc. Qin *et al*. [7] have studied dislocation and twinning mechanisms for DRX of as-cast Mn18Cr18N steel. The results show that at higher temperature and lower strain rate, DRX is controlled by dislocation slipping and climbing, but at higher strain rate and lower temperature, DRX is controlled by twins. Zhu *et al*. [8] have studied DRX mechanisms of Mn18Cr18N steel during hot deformation. The results show that both continuous dynamic recrystallization (CDRX) and discontinuous dynamic recrystallization (DDRX) exist in the hot deformation, and DDRX is the major mechanism. Wang *et al*. [9] have studied the effect of initial grain size on DRX and hot-ductility of Mn18Cr18N steel. The results show that the hot-ductility of Mn18Cr18N steel is very sensitive to grain size, especially at lower temperature. Coarse initial grains delay the occurrence and development of DRX, resulting in poor hot-ductility.

Previous researchers mainly focused on the characteristics of Mn18Cr18N steel itself, and the research on its hot deformation behavior and mechanism is relatively comprehensive. However, how to modify the characteristics of

✉ Corresponding authors: Yanwu Dong E-mail: dongyw@smm.neu.edu.cn; Zhouhua Jiang E-mail: jiangzh@smm.neu.edu.cn

Mn18Cr18N steel by some methods and further improve its hot deformation ability and optimize its hot deformation structure still need to be considered. It seems to be a feasible method to add some special elements (rare earth, magnesium, titanium, etc.) for microalloying, thereby modifying some characteristics of the steel [10–12].

Rare earth elements, widely used to modify properties of steel, have shown many unique characteristics. Firstly, rare earth elements are easily combined with O or S, so they can play an important role in deoxidizing, desulfurizing, and improving purity. Meanwhile, their oxides and sulfides are very stable, so they can modify Al_2O_3, MgO, MnS, and other inclusions into composite inclusions of rare earth oxides, rare earth sulfides and so on [13]. When the addition method and amount of rare earth elements are reasonable, the distribution of such inclusions tends to be fine and dispersed. In addition, some rare earth elements will dissolve in the metal matrix and play some special role [14]. Therefore, adding a proper amount of rare earth to steel has an impact on the mechanical properties, service properties and so on. However, there are few reports [15–16] about the effects of rare earth elements on hot deformation behavior of steel. Moreover, due to the complex existence of rare earth elements in steel, there is a lack of comprehensive and systematic research on the influence mechanism of rare earth elements on the hot deformation behavior of steel.

In this paper, Mn18Cr18N and Mn18Cr18N+Ce high nitrogen austenitic stainless steels were smelted. The effect of rare earth Ce on the hot deformation behavior of Mn18Cr18N steel was investigated by thermal compression tests. The main purpose is to explore the feasibility of improving the hot workability of Mn18Cr18N steel by adding rare earth, and to analyze its mechanism.

2. Experimental

In this paper, rare earth Ce was added to Mn18Cr18N steel by electroslag remelting in protective atmosphere (N_2). Mn18Cr18N steel produced by Pangang group Jiangyou Changcheng Special Steel Co., Ltd., China was used as consumable electrode. The composition of the slag was 40wt%CaF_2–16wt%CaO–20wt%Al_2O_3–4wt%MgO–20wt%CeO_2. Ca–Si was added as reducing agent in remelting process (5 g Ca–Si in 1 kg slag). Two kinds of steels with and without Ce were smelted, separately, and the composition is shown in Table 1.

Table 1. Composition of testing steels wt%

Type	Ce	Mn	Cr	Ni	C	Si	N	O	S	Fe
Mn18Cr18N	0	18.44	19.47	0.129	0.0946	0.300	0.495	0.0055	0.002	Bal.
Mn18Cr18N+Ce	0.0086	18.23	19.68	0.127	0.0963	0.289	0.497	0.0037	0.0003	Bal.

Specimens with 8 mm in diameter and 12 mm in height were machined from the half radius and half height of the ingot of the ingots, and axes of specimens are parallel to that of the ingots. Graphite sheets with a thickness of 0.25 mm were placed to reduce the friction between specimens and extrusion head, and tantalum sheets were placed to ensure uniform stress and thermal insulation of the specimen. The deformation temperatures were 1173, 1273, 1373, and 1473 K. The strain rates were 0.01, 0.1, 0.5 and 1 s^{-1}. The strain was 0.8. Firstly, the specimens were heated to 1523 K at a rate of 10 K/s and kept for 240 s, and then they were cooled to the deformation temperature at a rate of 5 K/s and kept for 30 s. Finally, the specimens were compressed at the corresponding strain rate to a strain of 0.8, which were water quenched immediately.

The deformed specimens were cut parallel to the compression axes. For optical microscope (OM) and electron probe microanalysis (EPMA) examinations, the specimens were first mechanically polished and then electrolytically etched (10vol% oxalic acid aqueous solution, 10 V, 40 s). For comparison, the as-cast specimens before compression were observed after chemical etching (0.1 g picric acid + 20 g $CuCl_2$ + 20 mL HCl + 40 mL C_2H_5OH + 80 mL H_2O, 3–8 s, cleaned with ammonia). Considering that the solidification of electroslag remelting is directional, the observation surface is parallel to the compression axes, and along the radius of ingots. For electron backscattered diffraction (EBSD) examinations, the specimens were treated by mechanical polishing, followed by argon ion bombardment for 90 min at 5 kV. For transmission electron microscope (TEM) examinations, the foils were achieved by grinding to a thickness of 50 μm followed by ion milling.

3. Results

3.1. Initial as-cast microstructure

The initial as-cast microstructure photos of Mn18Cr18N and Mn18Cr18N+Ce samples are shown in Fig. 1, where the typical dendrites are marked by yellow dash lines. It can be noted that the dendrite development of Mn18Cr18N is relatively complete, its secondary dendrite arm is long, and its secondary dendrite spacing is large. However, the dendrite development of Mn18Cr18N+Ce is incomplete, the secondary dendrite arm of which is very short, and the secondary dendrite spacing of which is small. The statistical results (30 fields for each sample) show that the secondary dendritic spacing is 64.9 and 54.2 μm for Mn18Cr18N and Mn18Cr18N+Ce steels, respectively, indicating that Ce can significantly refine the initial as-cast microstructure of Mn18Cr18N steel (about 16.5%).

3.2. Flow curves

Fig. 2 shows the flow curves of Mn18Cr18N steel and Mn18Cr18N+Ce steel. It can be noted that the peak stress

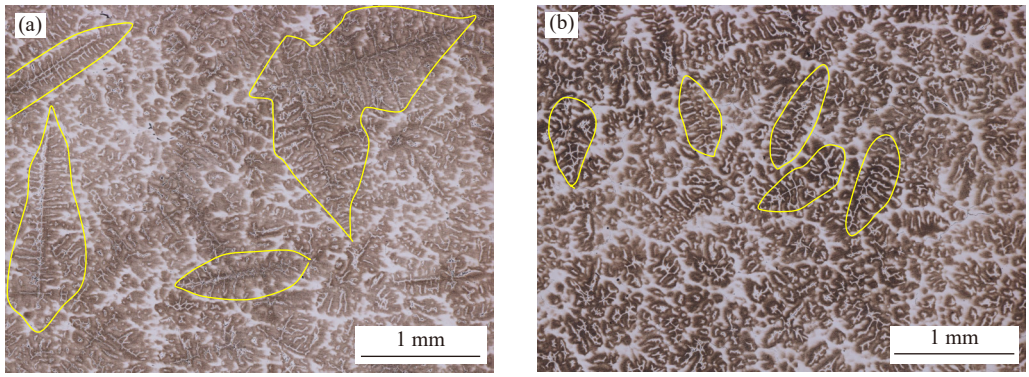

Fig. 1. Initial as-cast microstructures: (a) Mn18Cr18N; (b) Mn18Cr18N+Ce.

and the steady-state stress decrease with the increase of the deformation temperature and the decrease of the strain rate. The initial stage of deformation is work hardening stage. In this stage, the flow stress and the dislocation density increase rapidly, but the deformation storage energy is low. With the increase of the strain, the stress gradually approaches the peak value, which is uniform strain stage. On the one hand, under the action of heat activation and external force, the softening behavior caused by dynamic recovery (DRV) and DRX will appear. On the other hand, dislocations will intertwine with each other during movement, increasing the flow stress. With the further increase of the strain, the deformation storage energy further increases, and the softening effect counteracts the effect of work hardening. When they reach the dynamic equilibrium, the hot deformation process enters a smooth stage.

It can also be noted that Ce changes flow curves. At the low deformation temperature (1173–1373 K), Ce increases the peak stress and steady-state stress of Mn18Cr18N steel, but at the high deformation temperature (1473 K), the effect of Ce on the flow stress is not obvious.

3.3. Kinetic analysis

To further study the effect of Ce on the hot deformation behavior of Mn18Cr18N steel, the constitutive model needs to be established. The Arrhenius constitutive model not only considers the comprehensive influence of deformation conditions on hot deformation, but also better describes the steady-

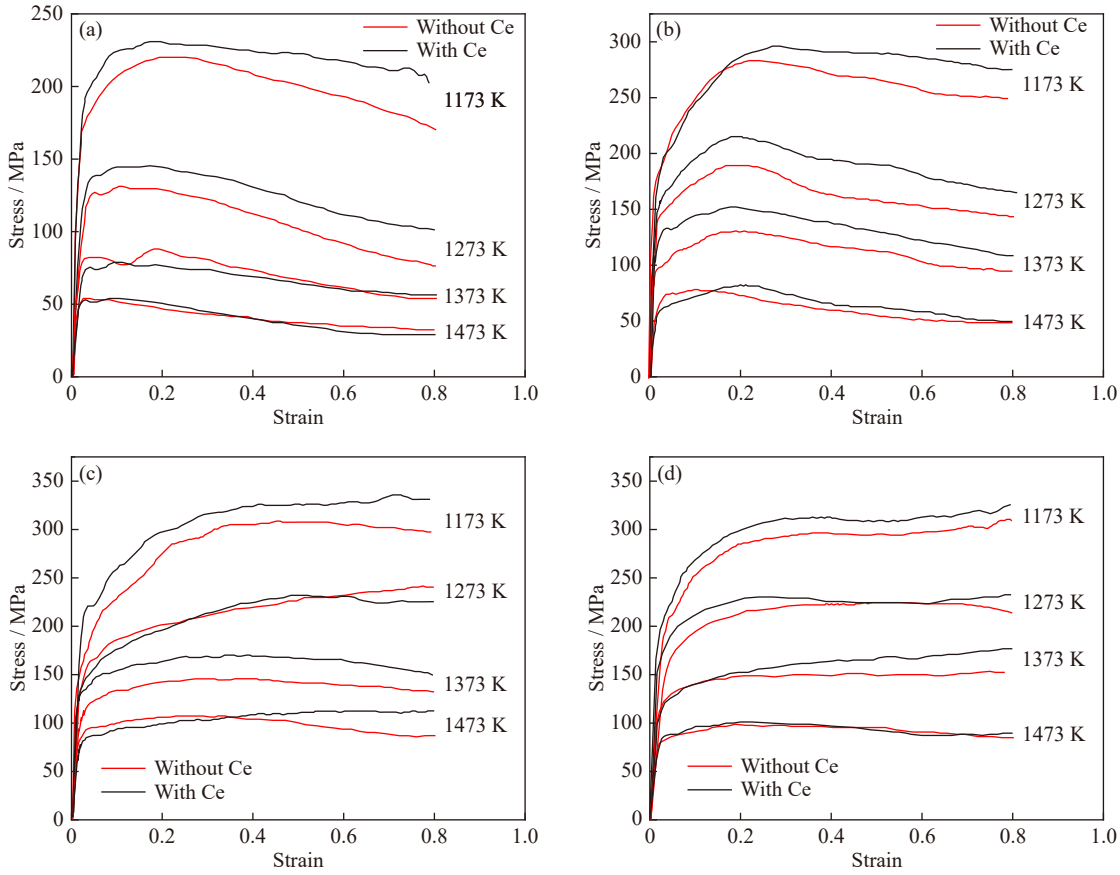

Fig. 2. Flow curves of Mn18Cr18N steel and Mn18Cr18N+Ce steel at different temperatures and strain rates: (a) 0.01 s^{-1}; (b) 0.1 s^{-1}; (c) 0.5 s^{-1}; (d) 1 s^{-1}.

tate deformation behavior of hot activation, which is the most widely used constitutive model [17]. The formulas used to solve the model are as follows:

$$Z = \dot{\varepsilon}\exp\left(\frac{Q}{RT}\right) \tag{1}$$

$$\dot{\varepsilon} = A_1\sigma^{n_1}\exp\left(\frac{-Q}{RT}\right) \tag{2}$$

$$\dot{\varepsilon} = A_2\exp(\beta\sigma)\exp\left(\frac{-Q}{RT}\right) \tag{3}$$

$$\dot{\varepsilon} = A[\sinh(\alpha\sigma)]^n\exp\left(\frac{-Q}{RT}\right) \tag{4}$$

$$\sigma = \frac{1}{\alpha}\ln\left\{\left(\frac{Z}{A}\right)^{\frac{1}{n}} + \left[\left(\frac{Z}{A}\right)^{\frac{2}{n}} + 1\right]^{\frac{1}{2}}\right\} \tag{5}$$

where Z is the Zener–Hollomon parameter, which can reflect the comprehensive effect of strain rate and deformation temperature on the flow behavior of alloys during hot deformation; Q is the activation energy of hot deformation (kJ·mol^{-1}); R is molar gas constant (8.314 J·mol^{-1}·K^{-1}); T is deformation temperature (K); A, A_1, A_2, n, n_1, α, and β are material constants, $\alpha = \beta/n_1$; σ is the flow stress (MPa); $\dot{\varepsilon}$ is the strain rate (s^{-1}).

In this paper, the peak stress was selected to calculate material constants and the activation energy. Taking Mn18Cr18N+Ce steel as an example, the logarithms on both sides of Eqs. (2), (3), and (4) are obtained respectively:

$$\ln\dot{\varepsilon} = \ln A_1 + n_1\ln\sigma - \frac{Q}{RT} \tag{6}$$

$$\ln\dot{\varepsilon} = \ln A_2 + \beta\sigma - \frac{Q}{RT} \tag{7}$$

$$\ln\dot{\varepsilon} = \ln A + n\ln[\sinh(\alpha\sigma)] - \frac{Q}{RT} \tag{8}$$

By plotting $\ln\dot{\varepsilon}$–$\ln\sigma$ and $\ln\dot{\varepsilon} - \sigma$ diagram (Fig. 3(a) and (b)), the average values of n_1 and β can be calculated as 5.53 and 0.0549, respectively, then $\alpha = \beta/n_1 = 0.00993$.

According to Eq. (8), the partial derivative of $\ln\dot{\varepsilon}$ (T = constant) and $1/T$ ($\dot{\varepsilon}$ = constant) is obtained:

$$n = \left\{\frac{\partial\ln\dot{\varepsilon}}{\partial\ln[\sinh(\alpha\sigma)]}\right\}_T \tag{9}$$

$$Q = R\left\{\frac{\partial\ln\dot{\varepsilon}}{\partial\ln[\sinh(\alpha\sigma)]}\right\}_T\left\{\frac{\partial\ln[\sinh(\alpha\sigma)]}{\partial(1/T)}\right\}_{\dot{\varepsilon}} = Rnl \tag{10}$$

By plotting $\ln\dot{\varepsilon}$–$\ln[\sinh(\alpha\sigma)]$ diagram (Fig. 3(c)), the value of n can be calculated as 4.984. Let $l = \partial\{\ln[\sinh(\alpha\sigma)]\}/\partial(1/T)$, by plotting $\ln[\sinh(\alpha\sigma)]$–$1000/T$ diagram (Fig. 3(d)), the value of l can be calculated as 12.761. Then, the activation energy of hot deformation can be calculated as 528.523 kJ·mol^{-1}. By plotting $\ln Z$–$\ln[\sinh(\alpha\sigma)]$ diagram (Fig. 3(e)), A can be calculated as 1.805×10^{18}.

Therefore, the hyperbolic sine constitutive equations of Mn18Cr18N+Ce steel at the peak stress are as follows:

$$Z = \dot{\varepsilon}\exp\left(\frac{528523}{RT}\right) \tag{11}$$

$$\sigma = 100.729\times\ln\left\{\left(\frac{Z}{1.805\times10^{18}}\right)^{\frac{1}{4.984}} + \left[\left(\frac{Z}{1.805\times10^{18}}\right)^{\frac{2}{4.984}} + 1\right]^{\frac{1}{2}}\right\} \tag{12}$$

Similarly, for Mn18Cr18N steel, it can be calculated that α = 0.00866, n = 5.746, Q = 499.099 kJ·mol^{-1}, and A = 2.601×10^{17}. The hyperbolic sine constitutive equations of Mn18Cr18N steel at the peak stress are as follows:

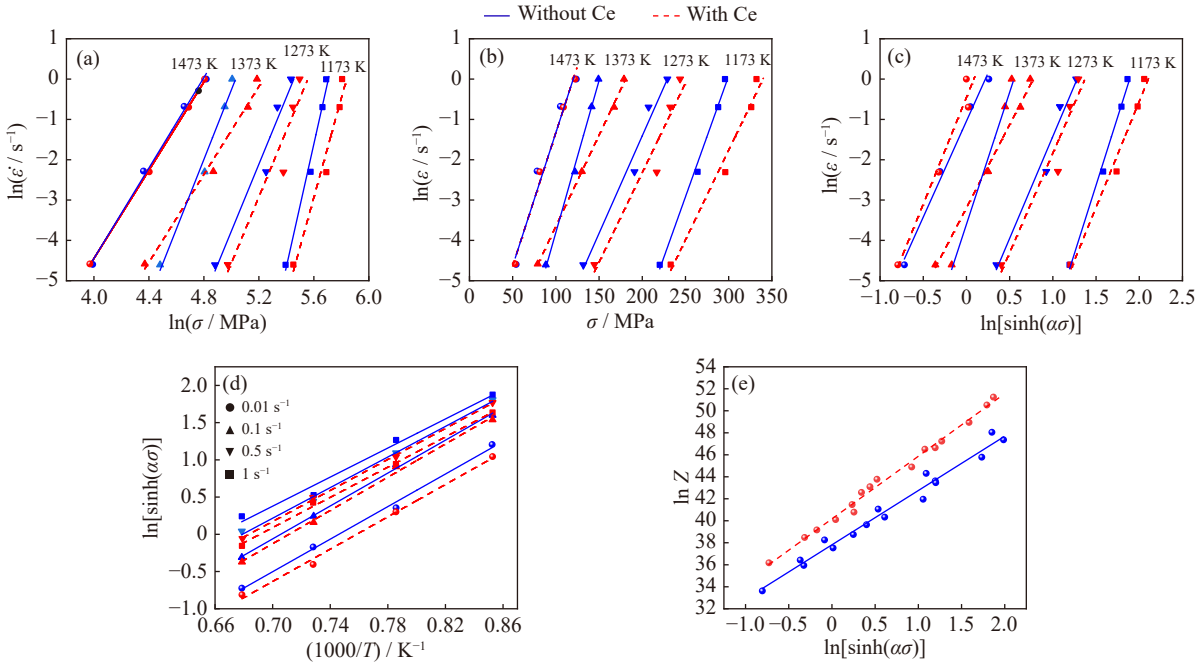

Fig. 3. Linear relationships between the physical quantities: (a) $\ln\dot{\varepsilon}$–$\ln\sigma$; (b) $\ln\dot{\varepsilon}$–σ; (c) $\ln\dot{\varepsilon}$–$\ln[\sinh(\alpha\sigma)]$; (d) $\ln[\sinh(\alpha\sigma)]$–$1000/T$; (e) $\ln Z$–$\ln[\sinh(\alpha\sigma)]$.

$$Z = \dot{\varepsilon} \exp\left(\frac{499099}{RT}\right) \tag{13}$$

$$\sigma = 115.47 \times \ln\left\{\left(\frac{Z}{2.601\times10^{17}}\right)^{\frac{1}{5.746}} + \left[\left(\frac{Z}{2.601\times10^{17}}\right)^{\frac{2}{5.746}} + 1\right]^{\frac{1}{2}}\right\} \tag{14}$$

Based on the above analysis, the hot deformation activation energy of Mn18Cr18N+Ce steel (528.523 kJ·mol^{-1}) is higher than that of Mn18Cr18N steel (499.099 kJ·mol^{-1}), indicating that the hot deformation resistance is improved after adding rare earth Ce.

3.4. Microstructure evolution

The microstructure photos of Mn18Cr18N+Ce steel at the same strain rate (0.1 s^{-1}) but different deformation temperatures are shown in Fig. 4(a), (b), (d), and (f). When the temperature is low (1173 K), coarse original grains are elongated along the compression direction, and fine DRX grains grow along the original grain boundaries, forming a typical necklace structure (Fig. 4(a)). With the increase of temperature, DRX grains gradually grow up. This is because the nucleation and growth of DRX grains are controlled by diffusion of atoms, and increasing temperature can accelerate the movement of atoms [18]. When the temperature reaches 1373 K, the microstructure of Mn18Cr18N+Ce steel is uniform and fine equiaxed grains (Fig. 4(d)), However, if the temperature is too high (1473 K), the grains are obviously coarsened (Fig. 4(f)).

The microstructure photos of Mn18Cr18N+Ce steel at the same deformation temperature (1373 K) but different strain rates are shown in Fig. 4(c), (d), and (e). When the strain rate is high (1 s^{-1}), although there are some uniform DRX grains in Mn18Cr18N+Ce steel (Fig. 4(c)), coarse original grains still exist in some region. This is because shorter deformation time leads to larger local deformation difference and incomplete DRX. With the decrease of strain rate, the degree of DRX gradually increases (Fig. 4(d)). This is because the lower strain rate provides sufficient time for grain boundary migration, which is conducive to the nucleation and grow of

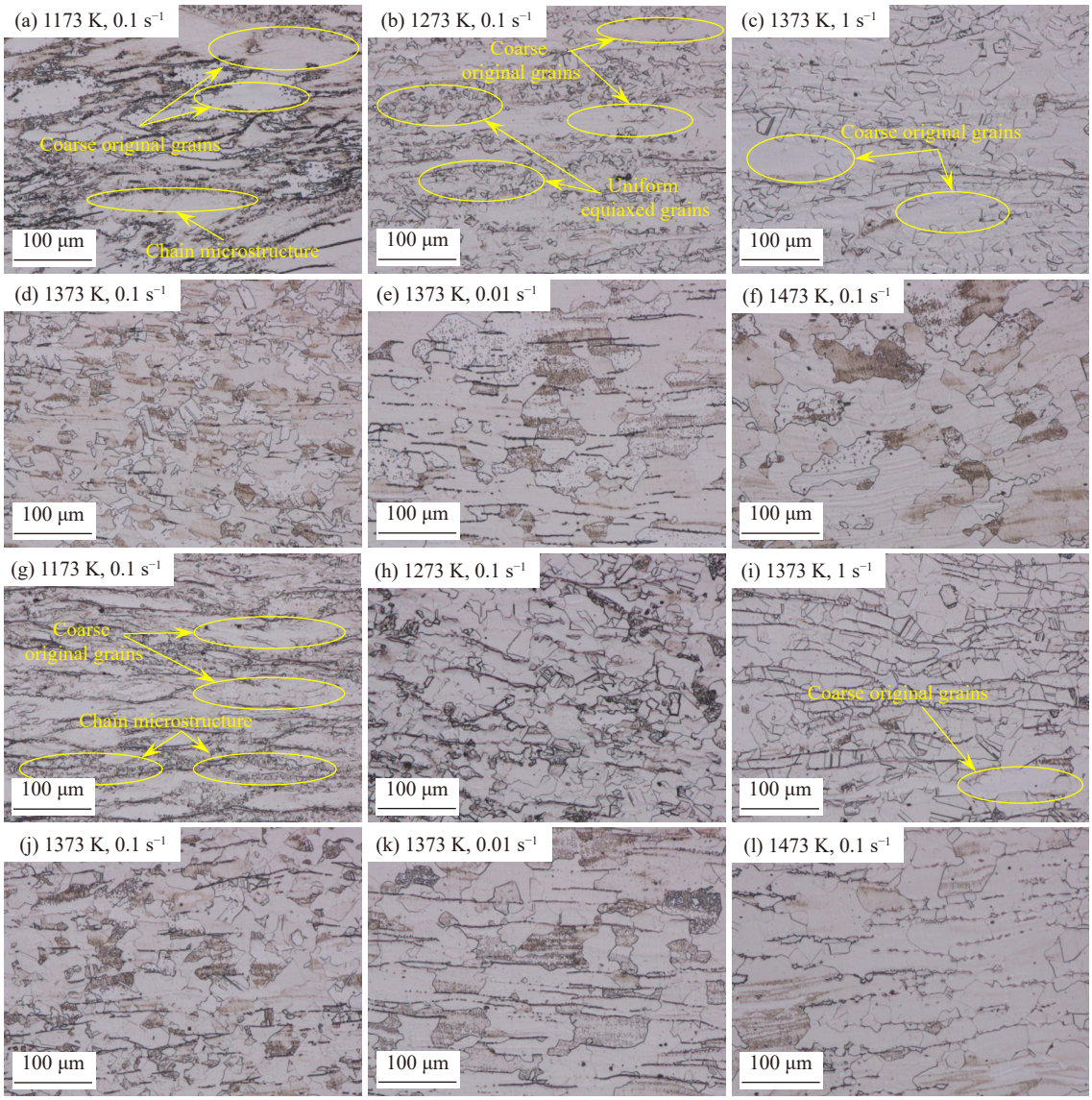

Fig. 4. Microstructure evolution during hot deformation: (a–f) Mn18Cr18N+Ce; (g–l) Mn18Cr18N.

DRX grains. However, if the strain rate is very low (0.01 s^{-1}), the deformation time is too long so that the DRX grains are obviously coarsened (Fig. 4(e)).

In addition, it can be noted that the microstructure evolution of Mn18Cr18N steel (Fig. 4(g)–(l)) is similar to that of Mn18Cr18N+Ce steel. However, the size of DRX grains is larger, indicating that Ce can inhibit the coarsening of DRX grains.

To study the effect of Ce on microstructure evolution more accurately, EBSD experiment was used to observe the deformation behavior of Mn18Cr18N and Mn18Cr18N+Ce steels under the conditions of 1173 K, 0.1 s^{-1} and 1373 K, 0.1 s^{-1}. Fig. 5 shows the orientation imaging microscopy (OIM) maps of the samples, where the low angle grain boundaries (LAGBs, <15°) are marked with green lines, the high angle grain boundaries (HAGBs, >15°) are marked with black lines, and the Σ3 twin grain boundaries (60°) are marked with red lines. Fig. 6 shows the corresponding DRX fraction.

When deformed at 1173 K and 0.1 s^{-1}, It can be observed from Fig. 5(a) and (c) that the original large grains of Mn18Cr18N+Ce steel and Mn18Cr18N steel are elongated, and there are many LAGBs in their interior. Meanwhile, the elongated original grains are surrounded by many fine DRX grains with HAGBs, forming necklace structure. In addition, it can be noted from Fig. 6 that DRX grain area fraction of Mn18Cr18N+Ce steel is larger than those of Mn18Cr18N steel (10.7% > 6.2%).

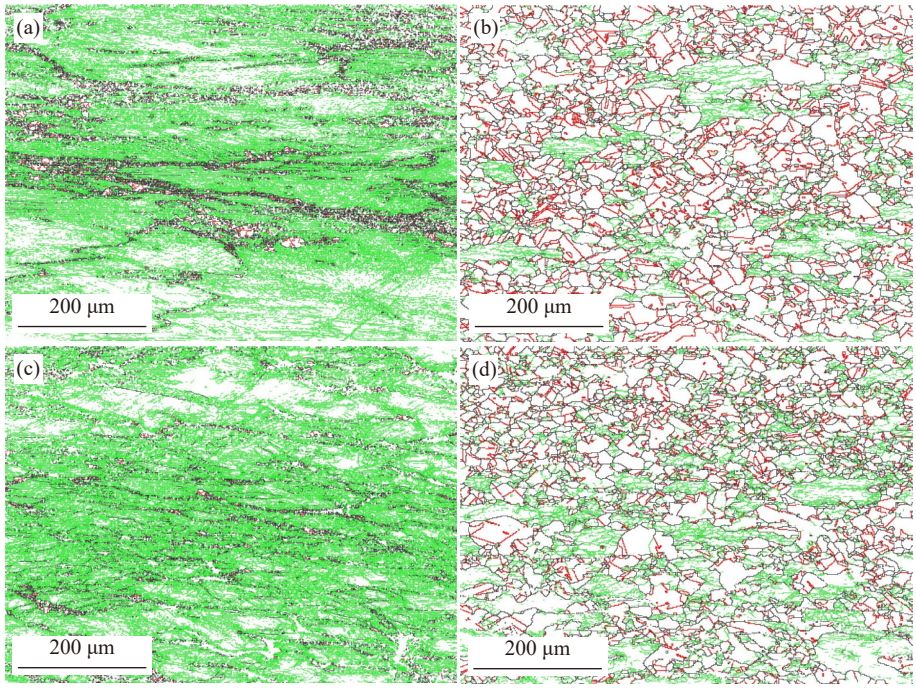

Fig. 5. OIM maps of the samples: (a) Mn18Cr18N+Ce, 1173 K, 0.1 s^{-1}; (b) Mn18Cr18N+Ce, 1373 K, 0.1 s^{-1}; (c) Mn18Cr18N, 1173 K, 0.1 s^{-1}; (d) Mn18Cr18N, 1373 K, 0.1 s^{-1}.

When deformed at 1373 K and 0.1 s^{-1}, the microstructure of Mn18Cr18N+Ce steel and Mn18Cr18N steel is relatively uniform, and only a few regions remain elongated large grains (Fig. 5(b) and (d)), the reason for which is the increase of deformation temperature promotes the growth of DRX grains and the disappearance of original large grains. It is noted that compared with Mn18Cr18N steel, the residual large grains in Mn18Cr18N+Ce steel are less; besides, the DRX area fraction (Fig. 6) are also larger (47.2% > 27.9%).

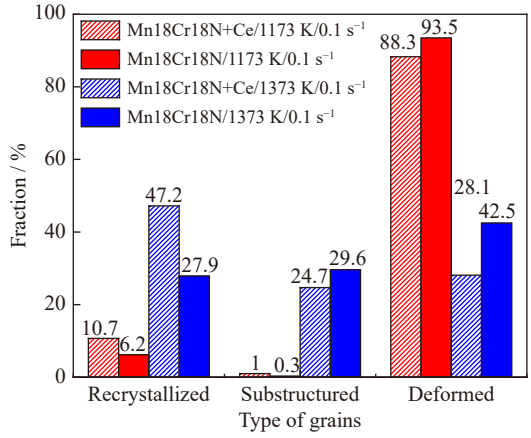

Fig. 6. Dynamic recrystallization fraction of the samples.

According to the above analysis of microstructure evolution, under different deformation conditions, the DRX grains of Mn18Cr18N+Ce steel are uniform and fine, and the DRX degree is always higher. It is fully proved that the addition of Ce can not only inhibit the growth of DRX grains, but also promote the development of DRX, which is beneficial to improve the hot workability. Some researchers [15–16] also observed the phenomenon of rare earth refining DRX grains and attributed it to solute drag effect, that is, the significant size difference between rare earth atom and matrix atom is beneficial to inhibit dislocation movement and grain boundary migration, thus delaying the emergence of DRX and in-

hibiting the growth of DRX grains. However, it should be noted that the solute drag effect not only inhibits the growth of grains, but also inhibits the emergence and development of DRX. In this paper, the degree of DRX is always higher after adding Ce. Therefore, it can be speculated that the existence of Ce improves the nucleation rate of DRX, because the two factors controlling the degree of DRX are growth rate and nucleation rate of DRX grains.

4. Discussion

Ce is very easy to combine with O or S to form inclusions and it will dissolve in the matrix. Therefore, the influence mechanism of Ce on hot deformation behavior should be analyzed from these two aspects.

4.1. Effect of Ce-containing inclusions on hot deformation behavior

4.1.1. Effect on hot deformation cracking

Generally, physical and chemical properties of inclusions and metal matrix, such as elasticity, plasticity and thermal expansion, are quite different. During the deformation, stress concentration occurs at the interface of inclusions and matric, which may lead to micro cracks. Micro cracks provide weak area for the destruction of materials, thereby deteriorating the workability [19–21].

The composition, quantity, and size of inclusions in Mn18Cr18N and Mn18Cr18N+Ce steels were counted by Aztec Steel module of SEM (Fig. 7). The results show that the number of inclusions in Mn18Cr18N steel is less (129.76 in 1 mm^2), but the size is obviously larger (the proportion of 0 < equivalent diameter (d) < 1 μm is only 27.62% but the proportion of $d \geq 3$ μm is 23.88%). The number of inclusions in Mn18Cr18N+Ce steel is more (164.00 in 1 mm^2), but most of them are fine and dispersed (the proportion of $0 < d < 1$ μm is up to 67.31% but the proportion of $d \geq 3$ μm is only 0.98%). Gao *et al.* [10] also observed that the proper amount of rare earth can promote the inclusions in steel to become uniform and dispersed, but with the increase of rare earth content, the inclusions will coarsen.

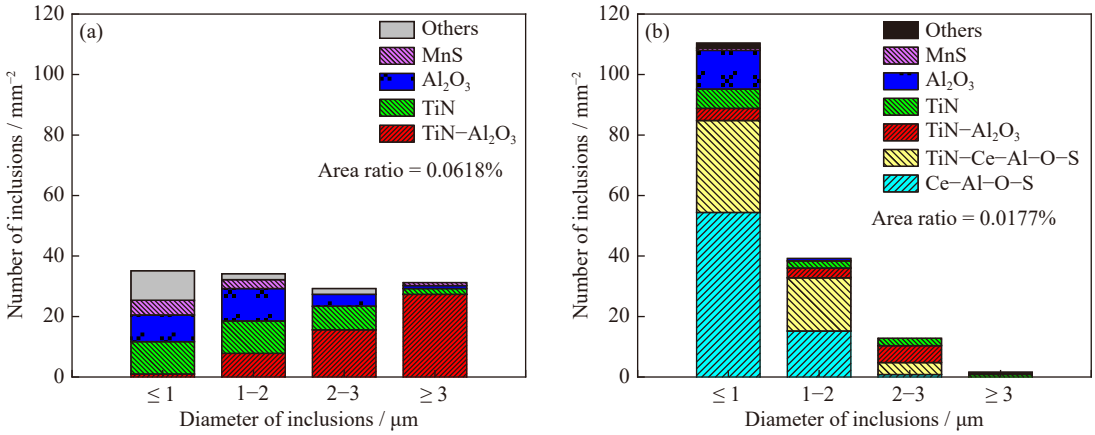

Fig. 7. Composition, quantity, and size of inclusions: (a) Mn18Cr18N; (b) Mn18Cr18N+Ce.

It can also be noted that the most typical inclusions in Mn18Cr18N steel are TiN–Al_2O_3, and the proportion of their quantity is 39.85%. Besides, there are many TiN (24.06%) and Al_2O_3 (18.80%). Such inclusions (Fig. S1) are large, angular, hard, and brittle [22]. Therefore, they will cause significant local stress during the hot deformation. On the one hand, the strength of the interface between such inclusions and matrix is very low, thus micro cracks are easy to appear [23]. On the other hand, such inclusions are easily crushed. After the inclusions are broken, micro gaps appear in the original positions. If the micro cracks or gaps near the inclusions expand further, the billet is easy to scrap. Especially at low temperature, high strain rate, and large strain, and the adverse effect is more serious.

However, after adding 0.0086% Ce, the proportion of TiN–Al_2O_3 (7.80%), TiN (7.32%), and Al_2O_3 (8.29%) is significantly reduced; thus, the adverse effect of them on hot deformation properties is weakened. Instead, most of inclusions in Mn18Cr18N+Ce steel are Ce-containing inclusions (74.64%). According to the differences of composition and structure, they can be divided into two types: Ce–Al–O–S (42.93%) and TiN–Ce–Al–O–S (31.71%). Yin *et al.* [11] studied the effects of Ce and Ti on the microstructure of steel and observed similar modification of Ce on (Ti/V) (C/N)–Al_2O_3 and Al_2O_3 inclusions.

Ce–Al–O–S inclusions (Fig. 8) are small in size and near–spherical in shape, besides, they have low hardness and high plasticity. Therefore, they will not cause significant local stress, decreasing the possibility of micro cracks and gaps formation and propagation. The structure of TiN–Ce–Al–O–S inclusions (Fig. 9) is similar to that of TiN–Al_2O_3 inclusions. Ce–Al–O–S inclusions are core and TiN inclusions are shell. Such inclusions have obvious edges and corners, but their size is much smaller than that of TiN–Al_2O_3. Therefore, though they can also cause stress concentration, the damage is very slight.

4.1.2. Effect on solidification structure

In addition, it is well known that some inclusions can be used as heterogeneous nucleation particles to induce grain nucleation, thus refining solidification structure [24–26]. The data in this paper also show that Ce can obviously refine the solidification structure of Mn18Cr18N steel. Therefore, it is

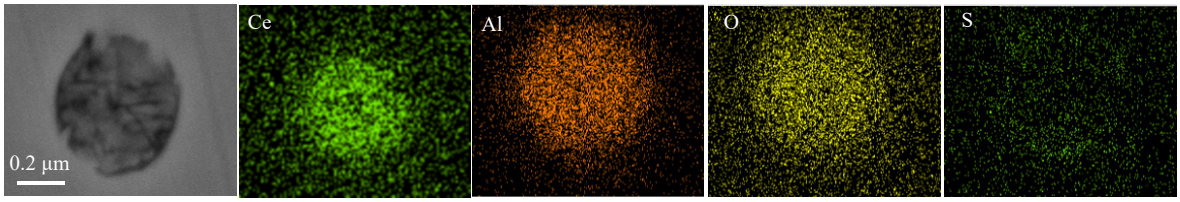

Fig. 8. Ce–Al–O–S inclusions in Mn18Cr18N+Ce steel.

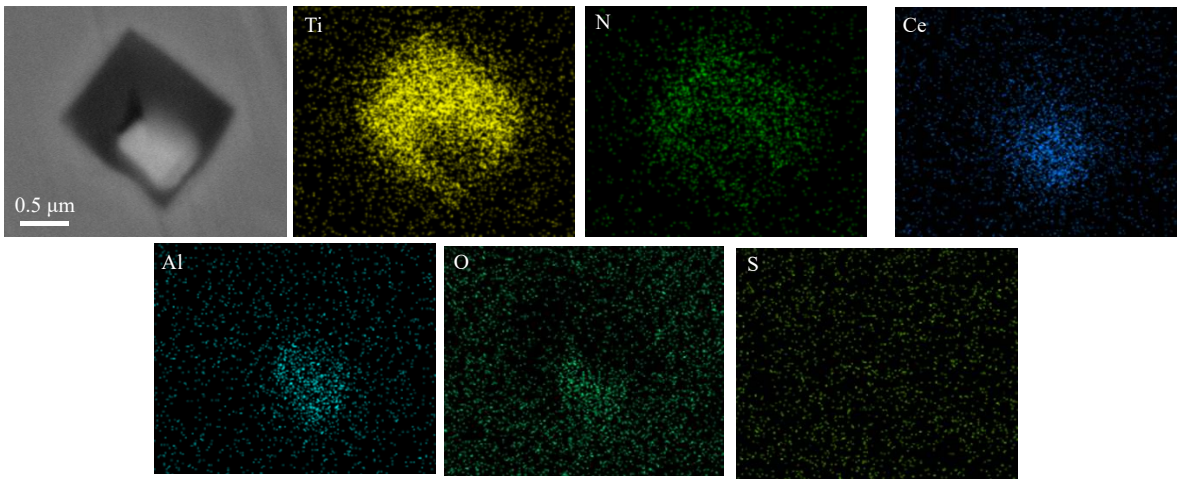

Fig. 9. TiN–Ce–Al–O–S inclusions in Mn18Cr18N+Ce steel.

necessary to analyze the effectiveness of Ce-containing inclusions as heterogeneous nucleation particles. Relevant studies [24,26] have mentioned that effective heterogeneous nucleation particles need to meet two conditions: (1) the melting point of particles is higher than that of metal matrix; (2) the lattice mismatch between particles and metal matrix is less than 12%, and the smaller the lattice mismatch, the easier the nucleation.

Generally, Ce-containing inclusions have higher melting points and exist in the form of solid particles in molten steel, that is, the first condition can be met. In addition, according to thermodynamic calculation, at liquidus temperature (1673 K) of Mn18Cr18N steel, the reaction liquid → δ occurs, further cooling to peritectic reaction temperature (1618 K), the reaction liquid + δ → γ occurs, after the end of peritectic reaction, the reaction δ → γ occurs. As long as the inclusions play a role of heterogeneous nucleation in reactions liquid → δ and liquid + δ → γ, as-cast γ grains can be refined, so it is necessary to consider the effect of inclusions on the nucleation of δ and γ together. The lattice mismatch of inclusions–δ or inclusions–γ can be calculated according to the Eq. (S1).

As a composite inclusion, the composition and lattice structure of Ce–Al–O–S are not constant, so it cannot be simply considered as a pure compound to calculate. In this paper, it is considered as a mixture of Al_2O_3, Ce_2O_3, and Ce_2O_2S (Since the content of S in Mn18Cr18N+Ce steel is only 0.0003%, pure sulfides of Ce are not considered). Therefore, it is necessary to calculate the lattice mismatch of Al_2O_3–δ, Al_2O_3–γ, Ce_2O_3–δ, Ce_2O_3–γ, Ce_2O_2S–δ, and Ce_2O_2S–γ respectively. On the contrary, though TiN–Ce–Al–O–S is also a composite inclusion, its TiN shell completely wraps the Ce–Al–O–S core, so the lattice mismatch of (TiN–Ce–Al–O–S)–δ and (TiN–Ce–Al–O–S)–γ equals the mismatch of the TiN–δ and TiN–γ, respectively. The calculation results (as shown in Table S1) indicates that the mismatch of Al_2O_3–δ and Al_2O_3–γ are larger than 12%, however, the mismatch of Ce_2O_3–δ, Ce_2O_2S–δ, Ce_2O_3–γ, and Ce_2O_2S–γ are far less than 12%. Therefore, although Al_2O_3 can't be used to heterogeneous nucleation particles, Ce–Al–O–S, as a mixture of Al_2O_3, Ce_2O_3, and Ce_2O_2S, may also play the role of heterogeneous nucleation in reactions of liquid → δ and liquid + δ → γ. Besides, the mismatch of TiN–δ is less than 12% but the mismatch of TiN–γ is larger than 12%, indicating that TiN–Ce–Al–O–S can be used as nucleation particles in reaction of liquid → δ, but not in reaction of liquid + δ → γ.

After as-cast γ grains refinement, the strength of the steel increases, thereby improving the hot deformation resistance and hot deformation activation energy [27]. Moreover, the grain boundary area increases, which can provide more favorable nucleation positions, thus improving the nucleation rate of DRX [18].

4.1.3. Effect on dislocation movement and grain boundary migration

In order to further analyze the effect of Ce-containing inclusions, micro characteristics of inclusions in hot compression samples of Mn18Cr18N+Ce steel were observed by TEM. From Fig. 10(a) and (b), many dislocations are entangled around the submicron inclusions at 1373 K and 0.1 s^{-1}, indicating that such fine and dispersed inclusions have a strong pinning effect on dislocation movement [28]. Therefore, they can play a role in dispersion strengthening and improve hot deformation resistance. Meanwhile, they can also inhibit the migration of grain boundaries, thus reducing the

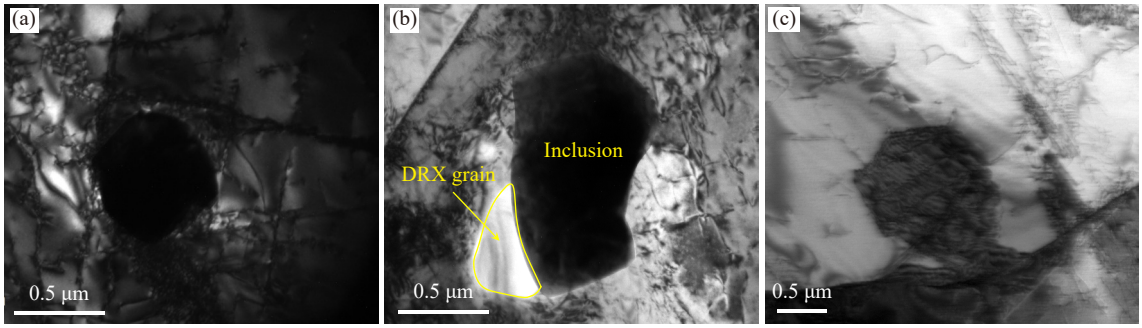

Fig. 10. TEM images of inclusions in Mn18Cr18N+Ce steel: (a, b) 1373 K, 0.1 s^{-1}; (c) 1373 K, 0.01 s^{-1}.

growth rate of DRX grains.

After decreasing the strain rate, the number of dislocations entangled near such inclusions will decrease (Fig. 10(c)). This is because the higher temperature provides more sufficient energy for the hot deformation, promoting the movement of dislocations and accelerating the annihilation of dislocations [29]; the lower strain rate increases the time of dislocation movement and annihilation. Therefore, the pinning effect on dislocation movement and the inhibition effect on grain growth are weakened.

In addition, it is noted that some DRX grains will nucleate around such fine dispersed inclusions (Fig. 10(b)). This is because the entangled dislocations around the inclusions may evolve into sub-grains after reaching a certain degree, and the sub-grains can grow into complete DRX grains by further absorbing the dislocations, which can be called particle-induced DRX [30]. This phenomenon shows that such fine dispersed inclusions are favorable nucleation points for DRX, which can improve the nucleation rate of DRX.

4.2. Effect of Ce segregation on hot deformation behavior

4.2.1. Effect on solidification structure

Compared with the heterogeneous nucleation, the solute effect may better explain the refinement of secondary dendrite [31]. Theoretically, due to the size of Ce atom (181.8 pm) is much larger than that of Fe atom (121.0 pm) and the melting point of Ce (1072 K) is much lower than that of Fe (1811 K), Ce atoms are extremely easy to enriched at the front of solid–liquid interface during solidification [14]. Moreover, in this paper, Ce atoms in molten steel are mainly transmitted by diffusion, the speed of which is so slow that Ce atoms cannot quickly leave. Therefore, a stable enrichment layer of Ce atoms may be formed at the front of the solid–liquid interface, and with the growth of dendrites, the enrichment becomes more and more obvious until a dynamic equilibrium is reached.

In this paper, EPMA was used to detect the trend of Ce content in as-cast Mn18Cr18N+Ce steel. The results (as shown in Fig. S2) show that the content of Ce in earlier solidification region (dendrite) is lower, while the content of Ce in the later solidification region (interdendrite and grain boundary) is higher, indicating that Ce atoms are indeed enriched in the front of solid–liquid interface.

With the enrichment of Ce atoms, the liquidus temperature of molten steel at the interface front decreases; however, the actual temperature gradient of molten steel is not affected. When the liquidus temperature gradient is greater than the actual temperature gradient, composition supercooling will occur [11]. The research of Zhang *et al.* [32] shows that there is a competitive relationship between adjacent secondary dendrites during the growth, that is, the fine secondary dendrites may be swallowed by the coarse secondary dendrites. The longer the stay time in the solid–liquid two phase region, the more sufficient the process is and the bigger the secondary dendrite is. However, the composition supercooling caused by Ce can obviously reduce the local solidification time, thus inhibiting the coarsening of secondary dendrite. After secondary dendrite refinement, the hot deformation resistance, the hot deformation activation energy, and the nucleation rate of DRX increase.

4.2.2. Effect on grain boundary migration

In addition, the nucleation and growth of DRX grains are closely related to the diffusion of atoms, but the diffusion ability of Ce atoms is obviously different from that of Fe atoms. Therefore, some DRX grains of hot compressed samples (1373 K, 0.01 s^{-1}) were randomly selected, and the contents of Ce at interior and boundaries of these grains were randomly detected by EPMA, as shown in Table 2.

Table 2. Content of Ce in boundary and interior of various grains in Mn18Cr18N+Ce hot compression sample wt%

Position	Grain 1	Grain 2	Grain 3	Grain 4	Grain 5
Boundary	0.025	0.027	0.009	0.062	0.022
Interior	0.016	0.017	0.000	0.000	0.000

The results show that for specific grains, the Ce content at grain boundary is larger than that at grain interior. Among different grains, the content of Ce at grain interior may also larger than that at grain boundary, such as No. 2 grain and No. 3 grain, which is mainly caused by position difference. If the grain nucleates at the dendrite, the Ce content is lower, but if the grain nucleates at the interdendrite or grain boundary, the Ce content is higher.

All in all, Ce will also segregate at grain boundaries during DRX. DRX is nucleation and growth process of grains, which is controlled by grain boundary migration [16]. However, Ce atoms segregated at grain boundaries can hinder the diffusion of matrix atoms at grain boundaries and improve the activation energy of austenite grain boundary

migration [33]. Therefore, in the process of hot deformation, Ce segregated at grain boundaries can inhibit the growth rate of DRX grains.

4.3. Microhardness

The main content of this paper is to study the effect of Ce on the hot deformation behavior of Mn18Cr18N steel. However, considering that the main purpose of hot deformation is to enhance the mechanical properties, and rare earth elements are beneficial to improve the mechanical properties of the steel [10,34], it is necessary to discuss the mechanical properties of the samples. In view of the small size of hot deformation samples, only the microhardness of the samples was tested (10 points for each sample), and the results are shown in the Fig. 11.

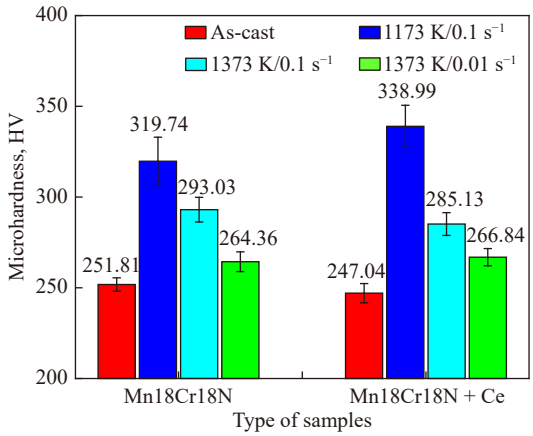

Fig. 11. Microhardness of as-cast and hot-deformed samples.

Before hot deformation, it is worth noting that the microhardness of as-cast Mn18Cr18N+Ce steel is slightly less than that of Mn18Cr18N steel, which is different from the results of hot deformation resistance in Fig. 2. This is because Ce can refine the as-cast microstructure, thus improving the hot deformation resistance of steel macroscopically. However, the as-cast grains after refinement are still very large, so it has little effect on the microhardness.

At 1173 K and 0.1 s^{-1}, the microhardnesses of both Mn18Cr18N and Mn18Cr18N+Ce steels increase significantly, the reason of which may include two aspects. Firstly, DRX has just occurred, and most areas of the samples are deformed original large grains containing many LAGBs in their interior, which can effectively improve the microhardness. Secondly, the size of DRX grain is much smaller than that of microhardness indentation, so it can play a significant role in fine grain strengthening. In addition, it is noted that the microhardness of Mn18Cr18N+Ce steel is much higher than that of Mn18Cr18N steel, which may be due to the finer DRX grains of Mn18Cr18N+Ce steel than those of Mn18Cr18N steel.

At 1373 K and 0.1 s^{-1}, the microhardnesses of both Mn18Cr18N and Mn18Cr18N+Ce steels decrease. This is because the DRX degree of both steels is higher and the DRX grains grow, so the contribution to microhardness decreases. In addition, the microhardness of Mn18Cr18N+Ce steel is lower than that of Mn18Cr18N steel. This is because the DRX degree of Mn18Cr18N+Ce steel is higher, and there are less deformed original grains containing LAGBs, the contribution of which to microhardness also decreases.

At 1373 K and 0.01 s^{-1}, the microhardnesses of both Mn18Cr18N and Mn18Cr18N+Ce decrease further and are very close. This is because the DRX of them under this condition is very sufficient and the size of DRX grain is much larger than the size of microhardness indentation, and the contribution of deformed original grains and fine DRX grains to microhardness no longer exists.

To sum up, compared with as-cast samples, the microhardness of hot–deformed samples increases significantly, and with the increase of DRX degree, the microhardness gradually decreases. In addition, the addition of Ce can affect the microhardness of Mn18Cr18N steel by affecting as-cast and hot deformation microstructures.

5. Conclusions

In this study, the influence of rare earth Ce on hot deformation behavior of as-cast Mn18Cr18N high nitrogen austenitic stainless steel was studied, and its influence mechanism was discussed. The main results are as follows:

(1) After adding rare earth Ce to Mn18Cr18N steel, the original inclusions (TiN–Al_2O_3, TiN and Al_2O_3) are modified into Ce-containing inclusions (Ce–Al–O–S and TiN–Ce–Al–O–S). Moreover, some Ce segregates at interdendrites and grain boundaries.

(2) During the solidification, Ce-containing inclusions can be used as effective heterogeneous nucleation particles to refine as-cast grains. Meanwhile, Ce atoms will enrich at the front of solid–liquid interface, reducing the local solidification time, thus refining the secondary dendrite. Therefore, the hot deformation resistance and activation energy are improved, and more favorable nucleation positions are provided for DRX.

(3) During the hot deformation, Ce-containing inclusions can inhibit dislocation movement and grain boundary migration, induce DRX nucleation, and avoid the formation and propagation of micro cracks and gaps. Meanwhile, Ce atoms tend to segregate at the boundaries of DRX grains, inhibiting the growth of grains.

(4) Compared with as-cast samples, the microhardness of hot-deformed samples increase significantly, and with the increase of DRX degree, the microhardness gradually decreases. In addition, Ce can affect the microhardness of Mn18Cr18N steel by affecting as-cast and hot deformation microstructures.

Acknowledgements

This work was financially supported by the National Natural Science Foundation of China (No. 51874084) and the Fundamental Research Funds for the Central Universities

(No. 2125026).

Conflict of Interest

The authors declare that no conflict of interest exists.

Supplementary Information

The online version contains supplementary material available at https://doi.org/10.1007/s12613-021-2355-6.

References

[1] C.H. Gao, T.L. Ren, and M. Liu, Low-cycle fatigue characteristics of $Cr_{18}Mn_{18}N_{0.6}$ austenitic steel under strain controlled condition at 100°C, *Int. J. Fatigue*, 118(2019), p. 35.

[2] H. Teuber, J. Barnikel, M. Dankert, W. David, A. Ghicov, and S. Voss, Development of a new high-strength steel for low pressure steam turbine end-stage blades, *J. Eng. Gas Turbines Power*, 141(2019), No. 1, art. No. 011021.

[3] C.Z. Zhao, S.S. Wei, Y.L. Gao, and Y.H. Wang, Progress of heat-resistant steel for supercritical and ultra-supercritical steam turbine, *J. Iron Steel Res.*, 19(2007), No. 9, p. 1.

[4] W.W. He, S.L. Sun, J.S. Liu, and H.G. Guo, Static recrystallization microstructure and model of Mn18Cr18N retaining rings steel, *Mater. Sci. Technol.*, 22(2014), No. 6, p. 17.

[5] W.W. He, J.S. Liu, Y.F. Guo, H.Q. Chen, and H.G. Guo, Microstructure evolution of multi-heats forging of Mn18Cr18N retaining ring steel and numerical simulation, *J. Plast. Eng.*, 17(2010), No. 2, p. 45.

[6] F. Li, H.Y. Zhang, W.W. He, H.Q. Chen, and H.G. Guo, Compression and tensile consecutive deformation behavior of Mn18Cr18N austenite stainless steel, *Acta Metall. Sin.*, 52(2016), No. 8, p. 956.

[7] F.M. Qin, H. Zhu, Z.X. Wang, X.D. Zhao, W.W. He, and H.Q. Chen, Dislocation and twinning mechanisms for dynamic recrystallization of as-cast Mn18Cr18N steel, *Mater. Sci. Eng. A*, 684(2017), p. 634.

[8] D.L. Zhu, M. Zhang, and Y. Wang, Electron backscattered diffraction study of microstructural evolution during isothermal deformation of high-N Mn18Cr18 alloy, *Metall. Mater. Trans. B*, 50(2019), No. 4, p. 1662.

[9] Z.H. Wang, S.H. Sun, B. Wang, Z.P. Shi, R.H. Zhang, and W.T. Fu, Effect of grain size on dynamic recrystallization and hot-ductility behaviors in high-nitrogen CrMn austenitic stainless steel, *Metall. Mater. Trans. A*, 45(2014), No. 8, p. 3631.

[10] J.Z. Gao, P.X. Fu, H.W. Liu, and D.Z. Li, Effects of rare earth on the microstructure and impact toughness of H13 steel, *Metals*, 5(2015), No. 1, p. 383.

[11] F.X. Yin, L. Wang, Z.X. Xiao, J.H. Feng, and L. Zhao, Effect of titanium and rare earth microalloying on microsegregation, eutectic carbides of M2 high speed steel during ESR process, *J. Rare Earths*, 38(2020), No. 9, p. 1030.

[12] Y. Huang, W.N. Liu, A.M. Zhao, J.K. Han, Z.G. Wang, and H.X. Yin, Effect of Mo content on the thermal stability of Ti–Mo-bearing ferritic steel, *Int. J. Miner. Metall. Mater.*, 28(2021), No. 3, p. 412.

[13] B. Šuler, J. Burja, and J. Medved, Modification of non-metallic inclusions with rare-earth metals in 50CrMoV13-1 steel, *Mater. Tehnol.*, 53(2019), No. 3, p. 441.

[14] H.Q. Hu, X.Y. Zhong, and H. Li, Influence of Ce on crystal morphology of austenite and dendritic segregation of Mn in high-Mn steel, *Acta Metall. Sin.*, 20(1984), No. 4, p. 247.

[15] N. Stanford, M.D. Callaghan, and B.D. Jong, The effect of rare earth elements on the behaviour of magnesium-based alloys: Part 1—Hot deformation behaviour, *Mater. Sci. Eng. A*, 565(2013), p. 459.

[16] H.H. Yan, Y. Hu, and D.W. Zhao, Influence of rare earth on dynamic recrystallization behavior of as-cast 30Mn steel, *Adv. Mater. Sci. Eng.*, 2018(2018), p. 8423415.

[17] A. Łukaszek-Sołek, T. Śleboda, J. Krawczyk, S. Bednarek, and M. Wojtaszek, Characterization of the workability of Ni–Fe–Mo alloy by complex processing maps, *J. Alloys Compd.*, 797(2019), p. 174.

[18] L.W. Xu, H.B. Li, Z.H. Jiang, M.H. Cai, W.C. Jiao, H. Feng, S.C. Zhang, and P.C. Lu, Hot deformation behavior of P550 steels for nonmagnetic drilling collars, *Steel Res. Int.*, 91(2020), No. 8, art. No. 2000035.

[19] Q.Y. Zang, Y.F. Jin, T. Zhang, and Y.T. Yang, Effect of yttrium addition on microstructure, mechanical and corrosion properties of 20Cr13 martensitic stainless steel, *J. Iron Steel Res. Int.*, 27(2020), No. 4, p. 451.

[20] X.Q. Pan, J. Yang, J. Park, and H. Ono, Distribution characteristics of inclusions along with the surface sliver defect on the exposed panel of automobile: A quantitative electrolysis method, *Int. J. Miner. Metall. Mater.*, 27(2020), No. 11, p. 1489.

[21] C. Gu, W.Q. Liu, J.H. Lian, and Y.P. Bao, In-depth analysis of the fatigue mechanism induced by inclusions for high-strength bearing steels, *Int. J. Miner. Metall. Mater.*, 28(2021), No. 5, p. 826.

[22] J.L. Lei, Z.L. Xue, H.Y. Zhu, and Y.D. Jiang, Research progress on non-metallic inclusion in tire cord steel for radial tire, *J. Iron Steel Res.*, 30(2018), No. 11, p. 847.

[23] A.L.V.D. Costa e Silva, The effects of non-metallic inclusions on properties relevant to the performance of steel in structural and mechanical applications, *J. Mater. Res. Technol.*, 8(2019), No. 2, p. 2408.

[24] B.L. Bramfitt, The effect of carbide and nitride additions on the heterogeneous nucleation behavior of liquid iron, *Metall. Trans.*, 1(1970), No. 7, p. 1987.

[25] M. Li, J.M. Li, D. Qiu, Q. Zheng, G. Wang, and M.X. Zhang, Crystallographic study of grain refinement in low and medium carbon steels, *Philos. Mag.*, 96(2016), No. 15, p. 1556.

[26] Y.C. Yu, S.H. Zhang, H. Li, and S.B. Wang, Effects of rare earth lanthanum on the solidification structure and hot ductility of Fe–43Ni expansion alloy, *High Temp. Mater. Process.*, 37(2018), No. 3, p. 261.

[27] M. El Wahabi, L. Gavard, F. Montheillet, J.M. Cabrera, and J.M. Prado, Effect of initial grain size on dynamic recrystallization in high purity austenitic stainless steels, *Acta Mater.*, 53(2005), No. 17, p. 4605.

[28] N. Choi, N. Park, J.K. Kim, A.V. Karasev, P.G. Jönsson, and J.H. Park, Influence of manufacturing conditions on inclusion characteristics and mechanical properties of FeCrNiMnCo alloy, *Metals*, 10(2020), No. 10, art. No. 1286.

[29] N. Nayan, S.V.S.N. Murty, S. Chhangani, A. Prakash, M.J.N.V. Prasad, and I. Samajdar, Effect of temperature and strain rate on hot deformation behavior and microstructure of Al–Cu–Li alloy, *J. Alloys Compd.*, 723(2017), p. 548.

[30] S.M. Lv, C.L. Jia, X.B. He, Z.P. Wan, Y. Li, and X.H. Qu, Hot deformation characteristics and dynamic recrystallization mechanisms of a novel nickel-based superalloy, *Adv. Eng. Mater.*, 22(2020), No. 12, art. No. 2000622.

[31] R. Schmid-Fetzer and A. Kozlov, Thermodynamic aspects of grain growth restriction in multicomponent alloy solidification, *Acta Mater.*, 59(2011), No. 15, p. 6133.

[32] J.B. Zhang, Y.C. Zhang, F. Zhang, D.X. Cui, Y.M. Zhao, H.X. Wu, X.Z. Wang, Q. Zhou, and H.F. Wang, Dendrite growth and grain "coarsening" in an undercooled CoNi equiatomic alloy, *J. Alloys Compd.*, 816(2020), art. No. 152529.

[33] Q.X. Yang, A. Wang, M. Gao, H.Q. Wu, and T.B. Guo, Effect of rare earth elements on austenite growth dynamics of steel 9Cr2Mo, *J. Iron Steel Res. Int.*, 3(1996), No. 1, p. 43.

[34] H. Wang, Y.P. Bao, M. Zhao, M. Wang, X.M. Yuan, and S. Gao, Effect of Ce on the cleanliness, microstructure and mechanical properties of high strength low alloy steel Q690E in industrial production process, *Int. J. Miner. Metall. Mater.*, 26(2019), No. 11, p. 1372.